Marine and Petroleum Geology 29 (2012) 143–151

Contents lists available at SciVerse ScienceDirect

Marine and Petroleum Geology

journal homepage: www.elsevier.com/locate/marpetgeo

The role of permeability evolution in fault zones on the structural and hydro-mechanical characteristics of shortening basins

Roozbeh Foroozan [a,b,*], Derek Elsworth [a], Peter Flemings [c], Frank Bilotti [d], Sankar Muhuri [d]

[a] Department of Energy and Mineral Engineering, Penn State University, University Park, PA 16802, USA
[b] Golder Associates Inc., Redmond, WA 98052, USA
[c] Department of Geological Sciences, University of Texas, Austin, TX, USA
[d] Chevron Corp., Houston, TX, USA

ARTICLE INFO

Article history:
Received 12 January 2011
Received in revised form
18 May 2011
Accepted 11 August 2011
Available online 17 September 2011

Keywords:
Permeability
Basin
Transport properties
Hydraulic fracture
Décollement
Faulting
Compaction

ABSTRACT

We examine the role of basin-shortening on the development of structural compartments in passive margin basins. A coupled flow-deformation model is used to follow the evolution of an idealized prismatic basin during lateral shortening. This includes the deformation-induced generation (lateral compaction) and dissipation (hydraulic fracturing) of pore fluid pressures and the resulting natural evolution of an underlying décollement and subsidiary fault structures. This model is used to examine the influence of strata stiffnesses, strain softening, permeability-strain dependence, permeability contrast between layers, and deformation rate on the resulting basin structure and to infer fluid charge within these structures. For a geometry with a permeability contrast at the base of the basin a basal décollement forms as the basin initially shortens, excess pore pressures build from the impeded drainage and hydrofracturing releases fluid mass and resets effective stresses. As shortening continues, thrust faults form, nucleating at the décollement. Elevated pore pressures approaching the lithostat are localized at the hanging wall boundary of the faults. Faults extend to bound blocks that are vertically offset to yield graben-like structural highs and lows and evolve with distinctive surface topography and separate pore pressure signatures. Up-thrust blocks have elevated fluid pressures and reduced effective stresses at their core, and down-thrust blocks the converse. The development of increased permeability on localized fault structures is a necessary condition to yield this up-thrust and down-thrust geometry. In the anti-physical case where evolution of permeability with shear strain is artificially suppressed, pervasive shear develops throughout the basin depth as fluid pressures are stabilized everywhere to the lithostat. Correspondingly, permeability evolution with shear is an important, likely crucial, feedback in promoting localization.

1. Introduction

Deformation patterns in active (Davis, 1996; Davis et al., 1983) and passive margins (Bilotti and Shaw, 2005) exhibit low-angle fault and fold structures where the geometry of deformation implicates the important role of low frictional strengths. Apparently-weak substrates may result from the presence of intrinsically weak and ductile materials such as salt or may evolve from the presence of overpressured fluids (Hubbert and Rubey, 1959). Décollement salt is implicated in gravitational spreading (Mourgues et al., 2009) in the Nile fan (Gaullier et al., 2000; Loncke et al., 2006), on the margins of Angola (Brun and Fort, 2004; Fort et al., 2004) and in the northern Gulf of Mexico (Rowan, 1997; Rowan et al., 2004; Wu et al., 1990) whereas sub-detachment overpressured shales promote deformation in the Niger Delta (Bilotti and Shaw, 2005; Briggs et al., 2006; Cohen and McClay, 1996; Corredor et al., 2005; Hooper et al., 2002; Weber and Daukoru, 1975), the Amazon fan (Cobbold et al., 2004) and the western Gulf of Mexico (Weimer and Buffler, 1992).

The response to sub-detachment salt is mechanically distinct from the response to overpressured shales. The rheology of salt is nearly constant with in situ effective stress and temperature whereas the mechanical strength of shale behavior is critically influenced by effective stress and hence the presence of excess pore pressures. Cello and Nur (1988) established that lithostatic pore pressures generated from transient poro-elastic loading and subsequent hydraulic fracturing is a suitable general model for the

* Corresponding author. FracMan Technology Group, Golder Associates Inc. 18300 NE Union Hill Road, Suite 200, Redmond, Washington, 98052, USA. Tel.: +1 (425) 883 0777, fax: +1 (425) 882 5498.
E-mail address: rforoozan@golder.com (R. Foroozan).

0264-8172/$ – see front matter © 2011 Elsevier Ltd. All rights reserved.
doi:10.1016/j.marpetgeo.2011.08.007

emplacement of shale fold and thrust belts. Pore pressures may be modified by a variety of mechanisms including rapid loading by sedimentation (Bethke, 1985) or lateral stress (Cello and Nur, 1988), clay dehydration (Osborne and Swarbrick, 1997), diagenesis (Yasuhara et al., 2003), thermal pressurization and expansion (Wibberley and Shimamoto, 2005), the production of hydrocarbons (Barker, 1990), coseismic shear heating (Hirose and Bystricky, 2007) and by changes in pore volumes or elevated rates of fluid transmission (Sibson, 2000, 2007). It is commonly accepted that the competition between mechanisms that either generate or dissipate pore pressures controls pore pressure history and hence the evolution of structure in deforming basins.

A variety of techniques have been applied to examine the role of fluid overpressures in deforming basins. These include physical models incorporating effective stress independent modeling materials such as silicone putty (Cobbold and Szatmari, 1991) and also methods involving stratification of permeability and the injection of scaled fluid pressures (Cobbold and Castro, 1999; R. Mourgues and Cobbold, 2006) to evaluate the role of effective stresses on deformation and the resulting structure. These methods typically employ the injection of air as the source of excess pore pressures and cannot replicate undrained changes in fluid pressure due to diagenesis, compaction, or changes in the composition of the solids or pore fluids. These effects can be accommodated in coupled numerical models. Early coupled models (the earliest being Gibson (1958)) assumed a relationship between the vertical effective stress and consolidation considering only uniaxial strain. In the geological community, publications by Bredehoeft and Hanshaw (1968), Smith (1971, 1973), Sharp (1976), Bethke (1985), and Wangen (1992) generalized this approach to geological systems and used numerical instead of analytical methods to solve for non-isothermal conditions. These works have been followed by a myriad of examples including Gordon and Flemings (1998) and Dugan and Flemings (2000).

Recently, more complicated numerical models have been used to accommodate the interaction of mechanical deformation and fluid flow using finite elements and finite difference methods which are not constrained to uniaxial strain (Ings and Beaumont, 2010; Matmon and Bekins, 2006; Morency et al., 2007; Saffer and Bekins, 2006; Strayer et al., 2001). These models generally study the faulting of a basin with geometric irregularities and generic models are rare (Sheldon et al., 2006). In this paper we explore the interplay between mechanisms that alternately generate (pore compaction and supply from a deforming substrate) and dissipate (fracturing and the development of strata traversing fluid flow conduits) pore fluid pressures in a shortening basin and examine the evolution and style of faulting and compartmentalization that results (Morency et al., 2007). Specific in our models and in contrast to previous representations we (1) incorporate large deformations and the effects of evolving topographic feedbacks (increased gravitational stresses) on the resulting basin structure, (2) presume no initial mechanical heterogeneity or pre-existing fault structures in the system, and (3) allow the mechanical detachment at a décollement and consequent faulting to develop naturally within the basin as a result of evolving fluid overpressures and feedbacks to effective stresses. Importantly, we show that permeability evolution due to up-migrating fracturing within the basin is a determining factor on the geometry and the pore pressure signatures of thrust structures.

2. Hydro-mechanical model

We select the simplest geometry possible to show that, contrary to many numerical models, geometrical irregularities are not required for the development of fold and thrust belts under tectonic compression. Rather, the development of faulting patterns and of fault-bounded compartments occurs naturally if sediment failure driven by fluid overpressures is systematically linked to an increase in permeability. This simple linkage, on its own, is capable of producing systematic structures within basins – as is explored in the following.

We consider a rectangular basin comprising a prism of sediments 5 km thick and 100 km wide that overlies a stiffer and more permeable substrate that is 15 km thick (Fig. 1). A variety of different process may contribute to the generation of pore pressures within a deforming basin, including mechanical compression, clay dehydration, diagenesis, shear heating and thermal expansion or fluid transmission from other regions. Our model does not distinguish between these various sources of pore pressure generation but uses lateral shortening of the 15 km-thick substrate as a generic representation of these processes. This substrate is a numerical-construct to develop broadly distributed and significant fluid mass fluxes that are representative of any of the previously noted mechanisms. This deeply-sourced fluid release then contributes to the evolving structure of the superstrate (basin) that is functionally independent of the fluid-source mechanism.

Mechanical and hydraulic characteristics of the sedimentary basin evolve with feedbacks as the strata are laterally compacted. The resulting deformation comprises contractional folds and deepwater thrusts common in passive-margin deltas (Rowan et al., 2004) and similar to structures of active margins (Davis, 1996; Davis et al., 1983). We consider our work to be a close analog to the contractional toe of the Niger Delta which is driven by the gravitational collapse of updip sediments (Bilotti and Shaw, 2005). These sediments detach along a décollement and transmit load to the deepwater sediment packages as a gross shortening of the structure.

The 2-D plane strain coupled hydro-mechanical model is solved using the finite difference code FLAC (Itasca, 2005). This method accommodates large strains during deformation without suffering a significant run-time penalty. Related pore volume changes drive

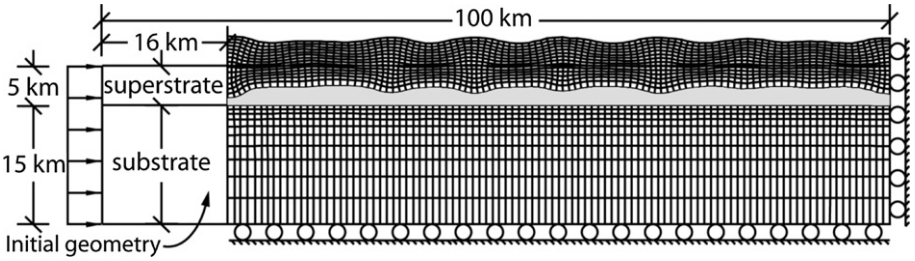

Figure 1. Initial geometry of model and the finite difference grid after 16% lateral deformation; Failure occurs at zero effective stresses at the décollement (gray shaded) due to insufficient dissipation of excess pore pressures. The substrate generates a constant upward flux that must be dissipated across the superstrate (basin). Where this flux is impeded by low permeability, fluid pressures build, effective stresses are reduced and the system is stabilized by the escape of fluid mass, the reduction in excess fluid pressures and the reestablishment of compactive effective stresses.

fluid expulsion and these are limited to volumetric strains with no influence on fluid pressures in shear-related deformation (which occurs in the elastic case without volume change). A denser grid will result in the evolution of thinner 'fault' zones but the spacing and the aspect ratios of the grid does not significantly change the orientation of localized deformation observed in this work (Strayer et al., 2001). Width and in some cases an orientation-dependence of shear localization to grid (FDM) and mesh (FEM) is a known issue in numerical modeling of shear band evolution (Itasca, 2005; Vermeer, 1990). The localization width is especifically important in this study as the strain localized within a shear band is inversely proportional to the band thickness. Subsequently, we will underline the qualitative description of the suggested mechanism for décollement/faults formation in passive margins.

2.1. Mechanical model

The geometry consists of a grid of 100 by 25 finite difference elements (Fig. 1). The upper 5 km superstrate has a much higher mesh density: a grid of 15 by 100. The lower 15 km of substrate has ten vertical nodes that fine toward the upper boundary. Boundary conditions consist of a free surface at the top and rollers at the bottom and to the right. The left boundary compresses both the substrate and superstrate at a rate of 10 cm/yr which is at the higher end for accretionary complexes (Saffer and Bekins, 2006). This shortening rate scales with the inverse of superstrate permeability – results would be similar for a tenfold-decrease in shortening rate coupled with a tenfold decrease in superstrate permeability. Drainage occurs only through the free surface. Initial conditions comprise hydrostatic pore pressures and equal vertical and horizontal stresses ($\sigma_v = \sigma_h$). Evolving conditions are insensitive to these initial conditions as lateral shortening develops a passive Rankine stress in the basin and the efflux of water from the substrate resets effective stresses in the superstrate (basin). Correspondingly, the effect of initial stress and pore pressure conditions on the results of later stages of deformation and resulting structure is minimal.

The 5 km thick superstrate is modeled as an elasto-plastic Mohr-Coulomb material with the properties noted in Table 1. The other elasto-plastic parameters of the model are chosen to capture the gross behavior of a contracting sedimentary basin. The choice of material properties to represent large scale behavior in a geomechanical model is challenging as the properties from laboratory-scale tests are not suitable for these models (Person et al., 1996). The strength and deformation parameters are chosen to generically represent foreland sediments and they are in the ranges suggested in the basin-scale modeling literature (Goodman, 1980; Simpson, 2009; Strayer et al., 2001). The substrate of the model (the lower 15 km) provides a broadly distributed, deep and controlled fluid efflux to the basin, as discussed previously. As such, it is assumed to be a poro-elastic solid that is also compressed by basin shortening.

Table 1
Hydro-mechanical properties of the models.

	Fluid	Substrate	Superstrate
Shear modulus (GPa)		14.4	0.77
Bulk modulus (GPa)	2	9.6 (4.8)[a]	1.7
Density (kg/m^3)	1000	2500	2500
Porosity		0.33	0.33
Initial permeability (m^2)		1.1×10^{-16}	1.1×10^{-17} (1.1×10^{-18})[a]
Permeability coefficient α			5 (10–100)[a]
Cohesion (MPa)			1 (0.01)[a]
Friction angle			30°
Dilation angle			0

[a] The values in parentheses are used in the parametric analyses.

To avoid the vertical expansion of the substrate during lateral compression the Poisson ratio is set to zero.

2.2. Hydraulic model

We assume linear Darcian flow within an equivalent porous medium. The basin is represented by a superstrate with initial parameters assumed constant with depth. This simplified assumption helps in the interpretation of the results presented later. The permeability of the substrate ($K_{sub} = 1.1 \cdot 10^{-16} m^2$) is one order of magnitude greater than the superstrate ($K_{sup} = 1.1 \cdot 10^{-17} m^2$) (Strayer et al., 2001), enabling excess pressures to build along the basal décollement which evolves naturally as a consequence of deformation. The superstrate (basin) permeabilities assumed here are representative of sedimentary shales in the higher end of the range suggested by Neuzil (1994) neglecting the influence of large scale evolving faults which may act as conduits at the basin-scale. For the near-steady conditions examined here (over geological timescales) the ratio of superstrate permeability to shortening rate controls the evolution of geometry in the system. As discussed later, high superstrate permeability requires high shortening rates (>5 cm/yr) in order to develop a décollement and subsequent faults.

Permeability of the superstrate is controlled by many factors including porosity, grain size, lithology, orientation of sediment layers relative to the flow field, deformation of strata, effective stress state, and fracturing or faulting (Saffer and Bekins, 2006). Here we focus our study on the impact of fracturing on permeability evolution in the fault zones. Conceptually, elevated permeabilities within fault zones are expected as the porosity increases by fracturing and dilation and new hydraulic connections are established. Permeability increases as large as 3 orders of magnitude have been reported (Faoro et al., 2009; Zhu and Wong, 1999) due to shearing. Mechanical compaction and also diagenesis over geological timescales further complicates the problem as permeability reduction up to 3 orders of magnitude can occur as a result of mineral precipitation (Polak et al., 2003; Schechte and Gidley, 1969). These competing processes may result in a fault with low permeability surrounded by a highly permeable damaged zone and fluid channeling along the fault (Barnicoat et al., 2009; Evans et al., 1997). In other words, the permeability of the faulting zone rock mass can be extremely anisotropic. In this study, as we will see, the dominant flow is along the faults and the assumption of isotropy is valid if the permeability assigned to the fractures is that relevant to the damaged zone. Permeability enhancement begins at the onset of microcracking and becomes increasingly important (Simpson et al., 2001). To incorporate the effect of shearing in our models, the permeability of the superstrate scales by a power law function with cumulative shear (Simpson et al., 2001, 2003)

$$\frac{K}{K_{ini}} = \begin{cases} \alpha^{(\gamma/\gamma_{th})^6} & \text{if } \gamma < \gamma_{th} \\ \alpha & \text{if } \gamma \geq \gamma_{th} \end{cases} \quad (1)$$

In the case of the reference model, $\alpha = 5$. Permeability remains constant at elevated shear strain magnitudes larger than the threshold strain($\gamma_{th} = 20\%$). Water is considered slightly compressible (Bulk modulus,$B_w = 2GPa$) in the fully coupled analyses performed and the porosity of both layers is 0.33. Results are not sensitive to the magnitude of the porosity of the system as advective fluxes and redistribution of heated fluids is not considered.

The coupled fluid-mechanical formulation (FLAC) comprises explicit time stepping between the fluid and mechanical timesteps with coupling between fluid and mechanical processes linked at each time step. The appropriate framework is that for the quasi-

static coupling via Biot theory (Biot, 1941; Itasca, 2005) where volume changes in the porous solid generate undrained fluid efflux that is redistributed by fluid transport within the porous medium. Fluid transport is described by Darcy's law where mass and momentum are conserved. The compressibility of grains is neglected compared to that of the drained bulk (Biot coefficient is unity) and the Biot modulus is the water bulk modulus divided by porosity. After each mechanical time step, a "*saturated fast-flow*" analysis is performed where the nodal pore pressures are incremented in proportion to the current unbalanced volume at a node (Itasca, 2005). The threshold values for unbalanced force (0.1 GN), average unbalanced volume (0.001) and maximum unbalanced volume (0.01) are set after checking the insensitivity of the results to further refinements.

3. Evolution of structure – gross response

With the geometry and mechanical characteristics of the basin defined we use this model to explore the evolution of structure within the superstrate as excess pore pressures control failure, fluid escape and the migration of zero effective stress effects upwards from the décollement. At the first stages of deformation (2%–6% lateral deformation) shear strains are mostly concentrated at the décollement and are of insufficient magnitude to significantly affect permeability (Fig. 2a, b). Effective vertical and horizontal stresses reach a maximum value and then decrease due to the development of increased pore water pressures at the décollement (Fig. 2a, Fig. 3). Pore water pressures initially build at the décollement where upwards migration is staunched by the low-permeability cap and only migrate upwards as fluid diffusion occurs. Similar pore pressure profiles have been observed in multiple natural basins (Morley et al., 2008). At larger deformations, shear strains at the décollement become focused as failure and localization occurs, resulting in increased permeability. This results in flow focusing along the fault structures as the vertical effective stresses approach zero at the décollement (Fig. 2a). Zones of cumulative shear strain concentration begin to develop upwards from the décollement at inclinations of about $45 - \phi/2$.

At 8% shortening (Fig. 2c, d), permeability increases in the deep portions of shear bands. Isolated islands of high effective stress form between adjacent shear zones. Tensional failure zones form at the décollement in response to the evolution of supra-lithostatic fluid pressures (zero vertical effective stress). These zones migrate upwards as pore water pressures equilibrate along faults due to their low hydraulic impedence and the low permeability of the surrounding matrix (Fig. 2c, e). The over-riding influence of excess pore fluid pressures in driving this response is evident when comparing the effective and total vertical stresses (σ_v) defined by the product of unit weight of saturated rock and depth below surface. Regions of near-zero effective stress represent zones of near-lithostatic fluid pressures and are located at the boundary between high and low permeability materials.

Further shortening (12%) allows the faults to reach their peak permeability ($K = 5K_{\mathrm{ini}}$) throughout their full length (Fig. 2g, h). Thus the faults act as conduits connecting deep permeable regions to the surface. Zones of zero effective stress are located at the boundary of permeable and impermeable materials on the hanging-wall side of the impermeable material because of water uplift force. Right-dipping faults are dominant in this case. The conjugate pair of left-dipping faults does not reach the surface, but a zone of zero effective stress is also apparent on the hanging wall of these deep undeveloped faults. At later stages of deformation (about 14% shortening), left-dipping faults reach the surface and isolate the relatively undeformed materials which they bound. These undeformed regions are located at the surface of up-thrust blocks and in the center of the down-dropped blocks (Fig. 2g, h).

Very high pore pressures (u) approaching lithostatic $\left(\lambda_{\min} = \left(\frac{u}{\sigma_v}\right)_{\min} \sim 0.8\right)$ permeate the full depth of the section and are seen in all of the stages of this model (Fig. 2g). The minimum value of λ occurs on the footwall at the boundary of the faults with the intervening blocks ($\lambda_{\min} = 0.8$) and the maximum ($\lambda_{\max} = 1$) occurs on the hanging wall.

The interplay of permeability evolution, pore pressure and faulting is better illustrated by considering vertical cross sections of vertical effective stress (Fig. 3). Early in the deformation history (6% shortening), lithostatic pore pressures build at the décollement due to the permeability contrast between the substrate and the superstrate. As shear deformations localize on the décollement, the permeability of the over-laying strata increases and a new permeability contrast boundary develops at the termination of this zone of failure. Since the hydraulic impedence of this flow conduit is low, lithostatic pore pressures are transmitted from depth to the tip of this zone which in turn results in further concentration of deformation and fault extension to shallower depths, as a positive feedback in the system. This is the essential mechanism controlling

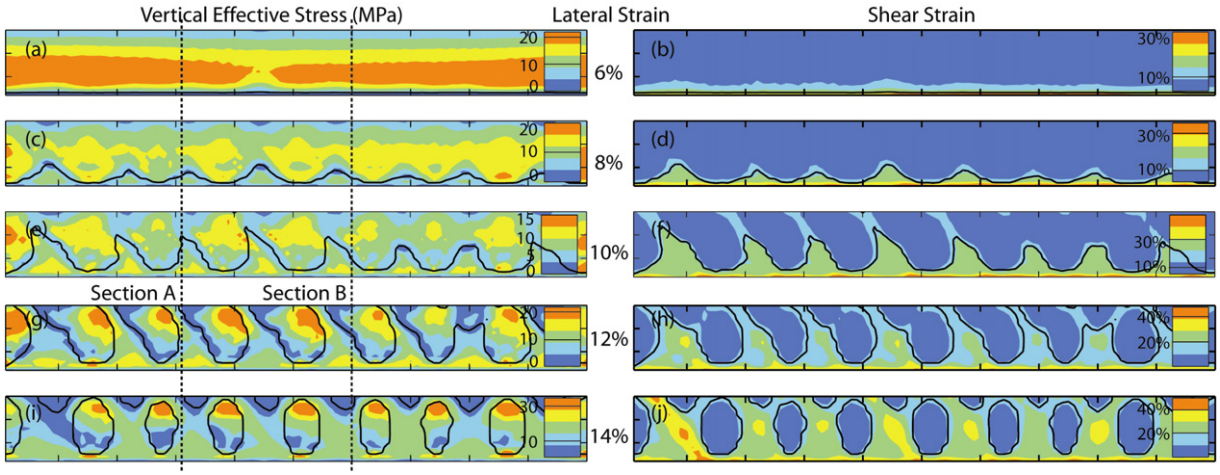

Figure 2. Vertical effective stress (left) and cumulative shear strain (right) contours for the reference model at 6%, 8%, 10%, 12% and 14% of lateral deformation. The single black line (a–j) is the permeability contour relevant to $(0.6\alpha)K_{\mathrm{ini}}$. For Sections A and B refer to Fig. 3. Only the superstrate is plotted (not to scale).

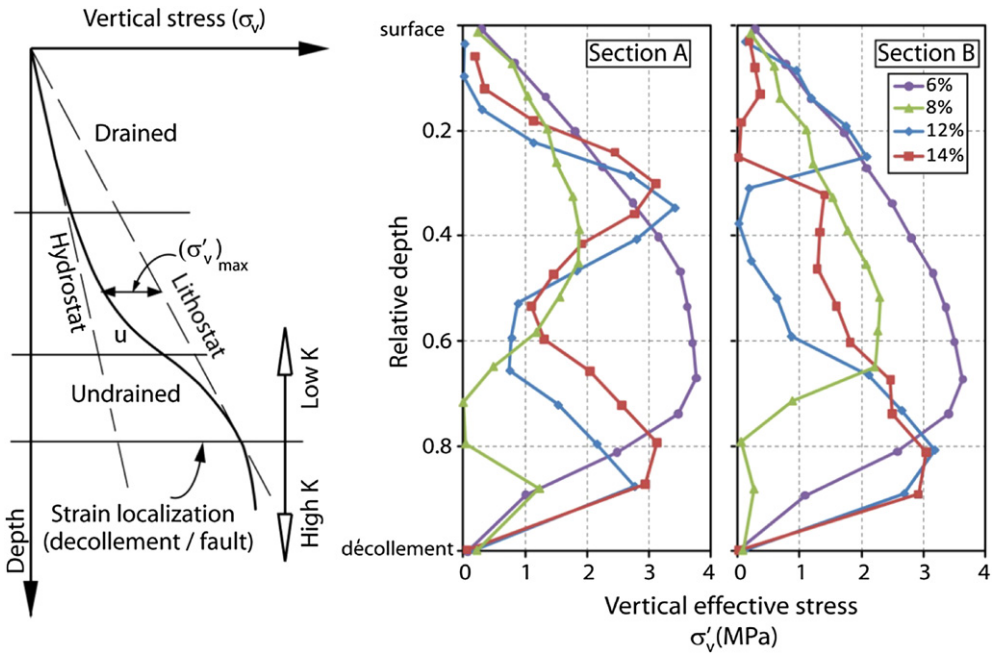

Figure 3. Schematic pore pressure (u) (left) and effective vertical stress (σ'_v) variation profile for sections (right) defined in Fig. 2. Thickening depth of the shortening basin is normalized by its maximum thickness. Strain localization occurs at the boundary of permeability contrast resulting in decreased effective stress and the early formation of the décollement and the later development of faulting.

the development of structure in these systems, and requires no *a priori* heterogeneity in material conditions (permeability or modulus or strength) nor of initial/boundary conditions.

4. Parametric analyses

The prior observations represent the generic response of the basin for defensible geometric and material properties. Specifically, it defined the crucial feedback of stress and fluid pressures on basin evolution, requiring only a single feature – that fracturing of the basin materials results in a small elevation in permeability that then allows the influence of fluid pressures to be projected further upwards through the sequence. In the following we investigate the role of various other influences on the form of the evolving basin. This influence is examined by varying a sequence of five conditions, with all other conditions remaining identical to those of the reference model. Through this, the respective roles of (1) substrate-superstrate relative stiffness, (2) strain softening in the superstrate (basin), (3) permeability-strain dependence of the basin material, (4) permeability contrast across the décollement, and (5) basin shortening rate are separately explored.

4.1. Substrate-superstrate relative stiffness

To examine the role of rate of fluid mass expulsion on the resulting evolution of structure in the basin, we decrease the substrate stiffness. The net fluid flux expelled from the substrate is decreased as the substrate stiffness is halved relative to the reference model ($E = 15\,GPa$). This redistributes an increasing shortening-induced load to the superstrate, decreases both stresses and volumetric compaction in the substrate, and reduces the fluid volume available for expulsion through the superstrate. Because of decreased pore pressures, at 2% deformation no shear strain localization is apparent at the detachment layer – localization is only apparent after 4% deformation. In general, the resulting evolution of structure is similar to the reference example but they are manifest later in the deformational history.

4.2. Strain softening

To examine the sensitivity of the model to strain softening of the material during shearing, cohesion is linearly reduced 90 percent from its initial value (1 MPa) to 10 kPa at 40% shear strain (Karacan et al., 2007). As a result, the final magnitude of cohesion at 16% lateral shortening of the basin is 10 kPa within the faults and about 0.7 MPa in the less deformed compartments. An important distinction between this model and the reference model is the extreme evolution of the right-dipping faults (Fig. 4a, b). From the early stages of deformation (8%), the right-dipping faults absorb the shortening-induced deformation at the expense of the conjugate set of left-dipping faults. This results from the effect of strain softening on strain concentration in the pre-deformed zones. Since in the reference model, the right-dipping faults develop first (due to the boundary conditions), these structures ultimately dominate through positive feedback enhanced by strain softening. With the same reasoning it can be concluded that diagenesis of the faulted zones with time will have the reverse effect of softening; resulting in more left-dipping faults than the reference case.

4.3. Permeability-strain dependence

The evolution of permeability during and after shear deformation is not well constrained. Hydraulic fracturing and shear fracturing exert different effects on the formation of fracture networks and the interplay of the mechanisms is complex (Barnhoorn et al., 2010; Cox, 2007, 2010). In the case of fluid pressure driven fractures, mineral precipitation can also greatly affect hydrologic properties which further complicates the relation (Min et al., 2009). Here we examine the effect of hydro-mechanical faulting-induced permeability evolution on the overall structural evolution of the deforming basin. To examine the sensitivity of the results to the parameterization of the shear–permeability relation, we vary the magnitude of the permeability multiplier for the superstrate from a factor of five in the reference model to a factor of ten ($\alpha = 10$). The resulting observations are:

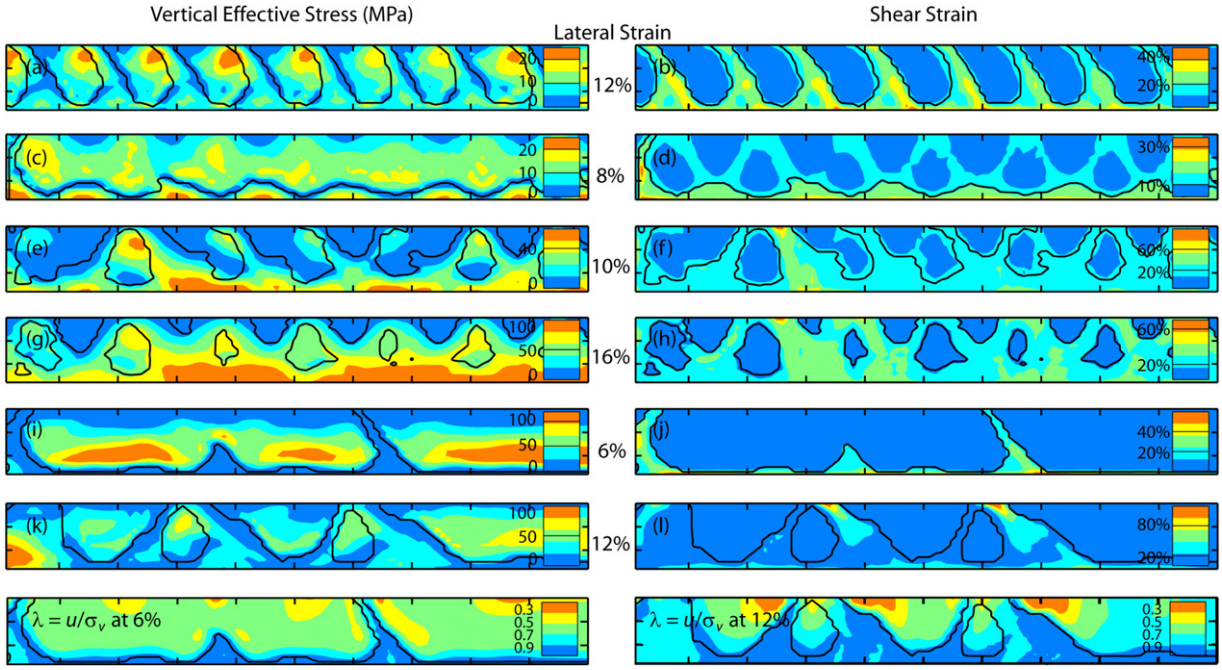

Figure 4. Vertical effective stress and cumulative shear strain contours for parametric studies: Strain Softening (10KPa $< C <$ 1MPa) (a, b), Permeability Dependence ($\alpha = 10$) (c–h), Permeability Contrast ($K_{sup} = K_{sub}/100$, $\alpha = 100$) (i–l). Bottom are the relative pore pressure (λ) contours for the Permeability Contrast model at 6% (left) and 12% (right) lateral strain. The single black lines in all graphs are the permeability contour relevant to $(0.6\alpha)K_{ini}$.

a) In the early stages (i.e., <8% shortening) shear strains concentrate in faults (Fig. 4c, d) and a distinct and irregular zone of zero effective stress forms over the décollement. This region is where the abrupt permeability change occurs due to larger shear strains at the décollement and deep faults (Fig. 3). The restricted efflux of water from highly permeable zones to the less-permeable zones is the cause of high pore pressures in the boundary region of the impermeable material.
b) At 10% shortening, fully-developed fault zones reach the surface (Fig. 4e, f). The dominant faults are right-dipping close to the deforming boundary and left-dipping close to the fixed boundary. Zones of zero vertical effective stress form the upper boundary of the faulted regions where there is a sudden decrease in permeability. Structurally, these are the deep regions of the hanging walls.
c) With further shortening low permeability zones are limited to the undeformed up-faulted blocks and to the central portions of down-faulted blocks which form from the intersecting fault zones (Fig. 4g, h). Due to the uplift force, the vertical effective stress is zero in the up-thrusted blocks. Since the faults act as drains in the system, the effective stresses are higher in the faults than in the surrounding zones.

The effects and observations mentioned are similar to the reference model but they exhibit a much stronger signature, confirming the role of permeability evolution on resulting structures.

4.4. Permeability contrast between substrate and superstrate

In this model, the permeability of the superstrate is decreased ten-fold to be 1/100th that of the substrate ($K_{sup} = 1.1 \cdot 10^{-18} m^2$). In this case, the fluid liberated by lateral shortening of the substrate redistributes hydrostatically within the substrate and is capped in magnitude to the lithostat at the décollement boundary. This dilates the lower portion of the superstrate (basin) and if it dissipates insufficiently quickly – it leads to unreasonable deformations at this boundary due to failure in extension (Fig. 1) unless the superstrate can release the overpressures by hydrofracturing. The permeability-enhancement rule of the superstrate is changed to accommodate this. The permeability-shear strain rule is modified so that at 20% shear strain the permeability is 100 times its initial value ($\alpha = 100$). In this case, major right-dipping faults separated by ~30 km form at 6% shortening (Fig. 4i, j). Since the permeability within these faults is elevated relative to the surrounding material, they act as drains connecting the deep décollement to the surface. On the hanging wall side of these faulted regions, the effective stresses are zero due to water uplift pressures exerted on the low permeability material. At larger deformations (Fig. 4k, l) right-dipping faults also develop and zones of high effective stress become separated by right and left-dipping faults. Elevated pore pressures approaching lithostat exist at the decollement and hanging walls (Fig. 4, bottom). The faults drain the excess pore pressure from the deep décollement and also the less-permeable materials in the hanging and foot walls.

4.5. Basin shortening rate

Shortening rate together with permeability evolution characteristics are the most important factors influencing the evolution of structural features and the redistribution of fluids in the basin. As the deformation rate decreases, pore water pressures accumulated in the substrate are able to dissipate. Thus vertical effective stresses at the zone of permeability contrast may not become zero (fluid pressures at lithostatic) and the décollement may not form at these sub-lithostatic fluid pressures. In this case, the entire vertical section of the superstrate and its lateral extent deforms uniformly without faulting and shear strains do not localize. This uniform distribution of shear strains results in less propensity to increase permeability, which consequently changes much less and with reduced feedback to the mechanical system. A minimum deformation rate is required to develop the décollement and subsequent faulting. In this case this threshold shortening rate is about 5 cm/yr, but can be adjusted relative to permeabilities and length scales of the system.

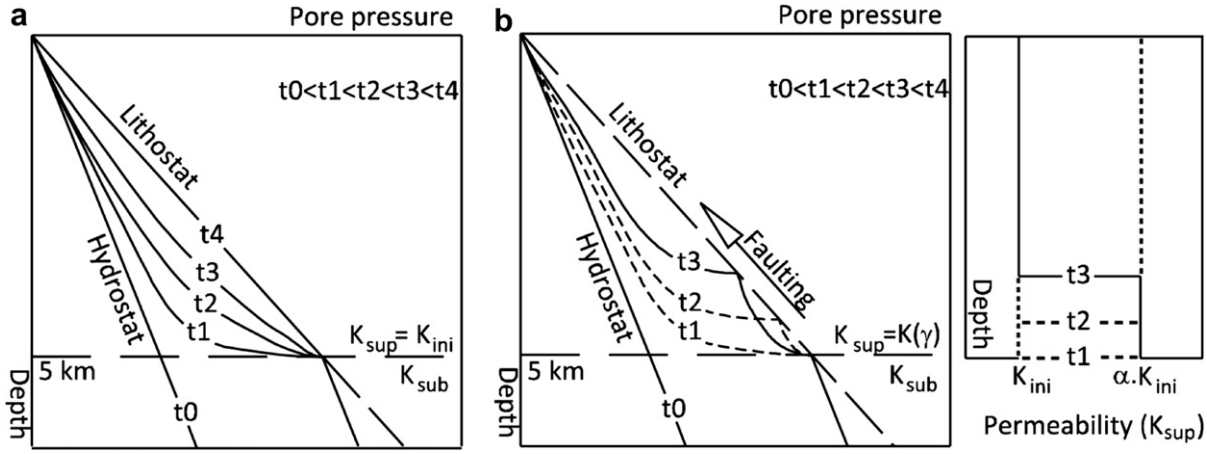

Figure 5. Schematic evolution of pore pressures for (a) constant permeability where the pore pressure is limited to the lithostat throughout the depth and (b) permeability evolves with shearing where the a lithostatic pore pressure limit migrates upwards due to hydrofracturing.

5. Summary and discussion

The suite of parametric models discussed in the preceding examines the role of excess water pressures on the evolution of a décollement at the interface of two layers with a permeability contrast and subsequent reverse faulting within a shortening basin. The décollement is able to form naturally as a result of the generated overpressures, in this case generated by mechanical compaction, but representative of other mechanisms, including for example chemical transformations and dehydration reactions. If permeability of the surface layer (K_{sup}) is artificially retained constant irrespective of shear strain, or if permeability increase due to shearing is too small, then at a dynamic steady state pore pressures evolve to the lithostat with no means to dissipate (Fig. 5a). Under this condition the effective stresses are everywhere zero, and pervasive deformation develops throughout the section, suppressing shear localization (faulting). Of course, this case is artificial, as there is no mechanism for pressure release. In contrast, the inclusion of a feasible strain-permeability law results in pore pressures which vary heterogeneously through the depth-section due to the propagation of faults. When the permeability evolves with shear strain ($K_{sup} = K(\gamma)$, Fig. 5b), the pore pressure is capped to the lithostat at the décollement and the topmost extent of the upwards migrating zone of enhanced permeability (Fig. 3). The zone of permeability contrast migrates up with further deformation (Fig. 5b-right). As a result the region of zero effective stress moves upwards from the initial décollement elevation (Fig. 5b-left, Fig. 2c, Fig. 4c). Further deformation results in the development of faults driven by lithostatic pore pressures (for exp. Fig. 2e, Fig. 3, Fig. 4a). This is in contrast with the constant permeability case (Fig. 5a) where no localization of the shear strains and faulting is observed in the model. Thus based on our numerical models, permeability evolution is a crucial factor in shear band localization of a homogenous medium without irregular boundary conditions.

Permeability change (hydrofracturing) is a mechanism for the escape of high pore pressures which cannot be accommodated otherwise in the sedimentary layer. This may be a factor determining the spacing of the faults as the spacing in the model with high permeability – shear strain dependency ($\alpha = 100$) is much larger than the previous cases ($\alpha = 5$ or 10).

Failure is concentrated at the top of this zero effective stress zone, and localizes on the extending fault. The extent of this zone depends on the magnitude of the permeability increase with shear strain. When the permeability becomes 5 times its initial value (due to shearing), maximum vertical effective stress in deep regions of the sedimentary basin is of the order of 15 MPa (at 10% shortening) which is much less than the vertical total stresses ($\sim$150 MPa) and the situation is not far from zero effective stress throughout the model (Fig. 2g, for instance). However, when the permeability is highly dependent on shear strain ($\alpha = 100$), the maximum vertical effective stresses are on the order of 50 MPa while the vertical effective stress on the décollement remains close to zero (representing fluid pressures at the lithostat) (Fig. 4e).

Formation of the décollement is crucial for the subsequent formation of the faulting zones (Fig. 3). In all of the cases modeled, shear strains are initially concentrated in the region of permeability contrast (décollement) due to the presence of elevated pore fluid pressures reaching the lithostat. Further shearing transfers the zone of permeability contrast to shallower levels and consequently the shear strains concentrates in the deep faults instead of at the initial décollement. This increase in permeability along the faults promotes the upward migration of the zone of zero effective stress and activates the shallower faults.

The shortening (compression) rate, the permeability of surface strata, the deformation properties of the substrate and the thickness of both layers are important factors influencing water expulsion and fluid pressure dissipation rates within the basin and subsequently in the formation of the décollement. For a given model geometry, permeability and deformation characteristics, there will be a threshold deformation rate below which no décollement and fault will form – rather excess fluid pressures dissipate as quickly as they form and shearing within the superstrate is pervasive rather than localized. Increased stiffness (elastic modulus) or depth of the substrate results in higher rates of water expulsion to the sedimentary layer and subsequently lower required deformation rates for the localization of deformation and the corresponding formation of décollement and faults. Conversely for a reduced permeability contrast between the two layers, the critical deformation rate will be greater.

The weakest zones of the sedimentary strata (with the least effective stresses) are generally located in the vicinity of the faulted zones on the boundary of hanging walls. Accordingly, elevated pore pressures in the hanging wall side of faults have been reported in natural formations (Eberhart-Phillips and Bannister, 2002; Manatschal, 1999). Because of the permeability contrast of the faulted and less deformed regions an uplift force is exerted on the hanging wall by the escaping water in the faults. Failure of the zones in extension at the permeability contrast boundary is a result

of this uplift force. Intrusive bodies of detrital materials, e.g., clastic injection plugs, dikes and sills, and extrusive features, e.g. detrital ridges, vents, and sheets, can develop in the hanging walls as a direct consequence of the hydrodynamic force applied due to permeability contrast (Voight, 1976). The zones of extension (zero effective vertical stress) migrate upwards as the deep fully-developed faults reach the surface. Inside the faults, partial drainage results in elevated effective stresses, relative to adjacent regions in the hanging walls (Fig. 4, bottom).

At very late stages of deformation, conjugate faults intersect and result in heavily faulted zones separating undeformed areas (Fig. 2j). Because of the uplift force exerted on the structural highs, the vertical effective stresses are zero in these regions while in lows the effective stresses are high because of drainage from the surrounding faults and the surface. In other words, the overlapping of hanging walls of adjacent right and left-dipping faults form the up-thrust blocks with high pore pressures and the footwalls form the down-thrust blocks. This explains why although both up-thrust and down-thrust blocks have experienced small shear strains and small changes in permeabilities, the down-thrust blocks have low pore pressures while the up-thrust regions have zero effective stresses.

In these models, right-dipping faults form preferentially in the earlier stages of deformation, due to boundary conditions, and remain dominant throughout basin shortening. Different boundary conditions including tapered base or surface, irregularities in the basal detachment or model height may also affect the developed structures (Gerbault et al., 1998; Panian and Wiltschko, 2007; Strayer et al., 2001). Regularly spaced faults are a common observation in passive margins as it is the case in the outer fold and thrust belt in the Niger Delta (Mourgues et al., 2009), Fanø Bugt glaciotectonic thrust complex (Andersen et al., 2005), or Larra thrust system (Teixell et al., 2000).

Early in the evolution, left-dipping faults only form at depth and terminate at their intersection with the right-dipping faults. Later, they may fully develop and reach the ground surface. By this time block cores maintaining their initial low permeabilities have been separated from each other as up-thrusted and down-thrusted blocks, respectively. Left-dipping faults are rather more frequent in the far right hand side of the model near the fixed boundary, and as such are viewed as a consequence of the boundary conditions. Once formed, the feedbacks of permeability, pore pressure migration, and work softening act to reinforce the existence of the earliest faults to develop, and these structures remain throughout all deformation.

Our model of a prismatic passive basin accommodates only a limited suite of behaviors. It does not take into account localization seeded by intrinsic inhomogeneities, irregular boundary conditions, horizontal fluid transport along the layering, the surcharge effects of sedimentation, nor of surface erosion. However, even without these features, it is able to show that the formation of a basal detachment and subsequent faulting is principally controlled by the coupling between permeability evolution and shear localization – indeed the two processes are intimately coupled with a strong first-order positive feedback. This study shows that permeability evolution not only affects the pore pressure signatures of the evolving basin, it also affects its structural features, such as the intensity and orientation of faults. These findings are unlikely to change with the addition of other second-order effects.

Acknowledgments

This work is a partial result of support by a gift from Chevron Co. This support is gratefully acknowledged. The conclusions reported here are those of the authors.

References

Andersen, L., Hansen, D., Huuse, M., 2005. Numerical modelling of thrust structures in unconsolidated sediments: implications for glaciotectonic deformation. Journal of Structural Geology, 587–596.
Barker, C., 1990. Calculated volume and pressure changes during the thermal cracking of oil to gas in reservoirs. Aapg Bulletin-American Association of Petroleum Geologists, 1254–1261.
Barnhoorn, A., Cox, S., Robinson, D., Senden, T., 2010. Stress- and fluid-driven failure during fracture array growth: implications for coupled deformation and fluid flow in the crust. Geology, 779–782.
Barnicoat, A., Sheldon, H., Ord, A., 2009. Faulting and fluid flow in porous rocks and sediments: implications for mineralisation and other processes. Mineralium Deposita, 705–718.
Bethke, C., 1985. A numerical model of compaction driven ground water flow and heat transfer and its application to paleohydrology of intracratonic basins. Journal of Geophysical Research-Solid Earth and Planets, 6817–6828.
Bilotti, F., Shaw, J.H., 2005. Deep-water Niger Delta fold and thrust belt modeled as a critical-taper wedge: the influence of elevated basal fluid pressure on structural styles. Aapg Bulletin 89 (11), 1475–1491.
Biot, M., 1941. General theory of three-dimensional consolidation. Journal of Applied Physics, 155–164.
Bredehoeft, J., Hanshaw, B., 1968. On the maintenance of anomalous fluid pressures: I. thick sedimentary sequences. Bulletin of the Geological Society of America 79, 1097–1106.
Briggs, S.E., Davies, R.J., Cartwright, J.A., Morgan, R., 2006. Multiple detachment levels and their control on fold styles in the compressional domain of the deepwater west Niger Delta. Basin Research 18 (4), 435–450.
Brun, J.P., Fort, X., 2004. Compressional salt tectonics (Angolan margin). Tectonophysics 382 (3–4), 129–150.
Cello, G., Nur, A., 1988. Emplacement of forland thrust systems. Tectonics, 261–271.
Cobbold, P.R., Szatmari, P., 1991. Radial gravitational gliding on passive margins. Tectonophysics 188 (3–4), 249.
Cobbold, P.R., Castro, L., 1999. Fluid pressure and effective stress in sandbox models. Tectonophysics 301 (1–2), 1–19.
Cobbold, P.R., Mourgues, R., Boyd, K., 2004. Mechanism of thin-skinned detachment in the Amazon Fan: assessing the importance of fluid overpressure and hydrocarbon generation. Marine and Petroleum Geology 21 (8), 1013–1025.
Cohen, H.A., McClay, K., 1996. Sedimentation and shale tectonics of the northwestern Niger Delta front. Marine and Petroleum Geology 13 (3), 313–328.
Corredor, F., Shaw, J.H., Bilotti, F., 2005. Structural styles in the deep-water fold and thrust belts of the Niger Delta. Aapg Bulletin 89 (6), 753–780.
Cox, S., 2007. Structural and isotopic constraints on fluid flow regimes and fluid pathways during upper crustal deformation: an example from the Taemas area of the Lachlan Orogen, SE Australia. Journal of Geophysical Research-Solid Earth.
Cox, S., 2010. The application of failure mode diagrams for exploring the roles of fluid pressure and stress states in controlling styles of fracture-controlled permeability enhancement in faults and shear zones. Geofluids, 217–233.
Davis, D., 1996. Accretionary Mechanics with Properties that Vary in Space and Time, Geophysical Monograph. Am. Geophys. Union.
Davis, D., Suppe, J., Dahlen, F.A., 1983. Mechanics of fold-and thrust belts and accretionary wedges. Journal of Geophysical Research 88 (NB2), 1153–1172.
Dugan, B., Flemings, P., 2000. The New Jersey margin: compaction and fluid flow. Journal of Geochemical Exploration, 477–481.
Eberhart-Phillips, D., Bannister, S., 2002. Three-dimensional crustal structure in the Southern Alps region of New Zealand from inversion of local earthquake and active source data. Journal of Geophysical Research-Solid Earth.
Evans, J., Forster, C., Goddard, J., 1997. Permeability of fault-related rocks, and implications for hydraulic structure of fault zones. Journal of Structural Geology, 1393–1404.
Faoro, I., Niemeijer, A., Marone, C., Elsworth, D., 2009. Influence of shear and deviatoric stress on the evolution of permeability in fractured rock. Journal of Geophysical Research-Solid Earth.
Fort, X., Brun, J.P., Chauvel, F., 2004. Salt tectonics on the Angolan margin, synsedimentary deformation processes. Aapg Bulletin 88 (11), 1523–1544.
Gaullier, V., Mart, Y., Bellaiche, G., Mascle, J., Vendeville, B.C., Zitter, T., Party, S.L.P.I.S., 2000. Salt Tectonics in and around the Nile Deep-sea Fan: insights from the PRISMED II Cruise. In: Geological Society London Special Publication, vol. 174.
Gerbault, M., Poliakov, A., Daignieres, M., 1998. Prediction of faulting from the theories of elasticity and plasticity: what are the limits? Journal of Structural Geology, 301–320.
Gibson, R., 1958. The progress of consolidation in a clay layer increasing with time. Geotechnique 8, 171–182.
Goodman, R.E., 1980. Introduction to Rock Mechanics. Wiley, New York.
Gordon, D., Flemings, P., 1998. Generation of overpressure and compaction-driven fluid flow in a Plio-Pleistocene growth-faulted basin, Eugene Island 330, offshore Louisiana. Basin Research, 177–196.
Hirose, T., Bystricky, M., 2007. Extreme dynamic weakening of faults during dehydration by coseismic shear heating. Geophysical Research Letters.
Hooper, R.J., Fitzsimmon, R.J., Grant, N., Vendeville, B.C., 2002. The role of deformation in controlling depositional patterns in the south-central Niger Delta, West Africa. Journal of Structural Geology 24 (4), 847–859.

Hubbert, M.K., Rubey, W.W., 1959. Role of fluid pressure in mechanics of overthrust faulting, I: mechanics of fluid-filled porous solids and its application to overthrust faulting. Geological Society of America Bulletin 70 (2), 115–166.
Ings, S.J., Beaumont, C., 2010. Continental margin shale tectonics: preliminary results from coupled fluid-mechanical models of large-scale delta instability. Journal of the Geological Society 167 (3), 571–582.
Itasca, 2005. Fast Lagrangian Analysis of Continua. Version 5.0 [computer program]. edited. Itasca Consulting Group, Inc, Minneapolis, Minn.
Karacan, C., Esterhuizen, G., Schatzel, S., Diamond, W., 2007. Reservoir simulation-based modeling for characterizing longwall methane emissions and gob gas venthole production. International Journal of Coal Geology, 225–245.
Loncke, L., Gaullier, V., Mascle, J., Vendeville, B., Camera, L., 2006. The Nile deep-sea fan: an example of interacting sedimentation, salt tectonics, and inherited subsalt paleotopographic features. Marine and Petroleum Geology 23 (3), 297–315.
Manatschal, G., 1999. Fluid- and reaction-assisted low-angle normal faulting: evidence from rift-related brittle fault rocks in the Alps (Err Nappe, eastern Switzerland). Journal of Structural Geology 21 (7), 777–793.
Matmon, D., Bekins, B., 2006. Hydromechanics of a high taper angle, low-permeability prism: a case study from Peru. Journal of Geophysical Research-Solid Earth.
Min, K., Rutqvist, J., Elsworth, D., 2009. Chemically and mechanically mediated influences on the transport and mechanical characteristics of rock fractures. International Journal of Rock Mechanics and Mining Sciences, 80–89.
Morency, C., Huismans, R.S., Beaumont, C., Fullsack, P., 2007. A numerical model for coupled fluid flow and matrix deformation with applications to disequilibrium compaction and delta stability. Journal of Geophysical Research-Solid Earth 112 (B10), 25.
Morley, C., Tingay, M., Hillis, R., King, R., 2008. Relationship between structural style, overpressures, and modern stress, Baram Delta Province, northwest Borneo. Journal of Geophysical Research-Solid Earth.
Mourgues, R., Cobbold, P.R., 2006. Thrust wedges and fluid overpressures: Sandbox models involving pore fluids. Journal of Geophysical Research-Solid Earth 111 (B5).
Mourgues, R., Lecomte, E., Vendeville, B., Raillard, S., 2009. An experimental investigation of gravity-driven shale tectonics in progradational delta. Tectonophysics, 643–656.
Neuzil, C., 1994. How permeable are clays and shales. Water Resources Research, 145–150.
Osborne, M.J., Swarbrick, R.E., 1997. Mechanisms for generating overpressure in sedimentary basins: a reevaluation. Aapg Bulletin 81 (6), 1023–1041.
Panian, J., Wiltschko, D., 2007. Ramp initiation and spacing in a homogeneous thrust wedge. Journal of Geophysical Research-Solid Earth.
Person, M., Raffensperger, J., Ge, S., Garven, G., 1996. Basin-scale hydrogeologic modeling. Reviews of Geophysics, 61–87.
Polak, A., Elsworth, D., Yasuhara, H., Grader, A., Halleck, P., 2003. Permeability reduction of a natural fracture under net dissolution by hydrothermal fluids. Geophysical Research Letters.
Rowan, M.G., 1997. Three-dimensional geometry and evolution of a segmented detachment fold, Mississippi Fan foldbelt, Gulf of Mexico. Journal of Structural Geology 19 (3–4), 463–480.
Rowan, M.G., Peel, F.J., Vendeville, B.C., 2004. Gravity-driven fold belts on passive margins. In: McClay, K.R. (Ed.), Thrust Tectonics and Hydrocarbon Systems. AAPG Memoir, pp. 157–182.
Saffer, D., Bekins, B., 2006. An evaluation of factors influencing pore pressure in accretionary complexes: implications for taper angle and wedge mechanics. Journal of Geophysical Research-Solid Earth.
Schechte, R., Gidley, J., 1969. Change in pore size distribution from surface reactions is porous media. Aiche Journal, 339.
Sharp, J., 1976. Momentum and energy balance equations for compacting sediments. Mathematical Geology 8, 305–322.
Sheldon, H., Barnicoat, A., Ord, A., 2006. Numerical modelling of faulting and fluid flow in porous rocks: an approach based on critical state soil mechanics. Journal of Structural Geology, 1468–1482.
Sibson, R., 2000. Fluid involvement in normal faulting. Journal of Geodynamics 29 (3–5), 469–499.
Sibson, R., 2007. An episode of fault-valve behaviour during compressional inversion? The 2004 M(J)6.8 Mid-Niigata Prefecture, Japan, earthquake sequence. Earth and Planetary Science Letters, 188–199.
Simpson, G., 2009. Mechanical modelling of folding versus faulting in brittle-ductile wedges. Journal of Structural Geology, 369–381.
Simpson, G., Gueguen, Y., Schneider, F., 2001. Permeability enhancement due to microcrack dilatancy in the damage regime. Journal of Geophysical Research-Solid Earth 106 (B3), 3999–4016.
Simpson, G., Gueguen, Y., Schneider, F., 2003. Analytical model for permeability evolution in microcracking rock. Pure and Applied Geophysics, 999–1008.
Smith, J., 1971. The dynamics of shale compaction and evolution of pore fluid pressure. Mathematical Geology (3), 239–263.
Smith, J., 1973. Shale compaction. Journal of Society of Petroleum Engineers 13, 12–22.
Strayer, L., Hudleston, P., Lorig, L., 2001. A numerical model of deformation and fluid-flow in an evolving thrust wedge. Tectonophysics, 121–145.
Teixell, A., Durney, D., Arboleya, M., 2000. Stress and fluid control on décollement within competent limestone. Journal of Structural Geology, 349–371.
Vermeer, P., 1990. The orientation of shear bands in biaxial tests. Geotechnique, 223–236.
Voight, B. (Ed.), 1976. Mechanics of Thrust Faults and Decollement. Dowden, Hutchinson & Ross, Inc., Stroudsburg, PA, p. 471.
Wangen, M., 1992. Pressure and temperature evolution in sedimentary basins. Geophysical Journal International, 601–613.
Weber, K.J., Daukoru, E.M., 1975. Petroleum Geology of the Niger Delta, paper presented at Ninth World Petroleum Congress. Applied Science Publishers, Ltd., London.
Weimer, P., Buffler, R.T., 1992. Structural geology and evolution of the Mississippi fan fold belt, deep Gulf of Mexico. Aapg Bulletin-American Association of Petroleum Geologists 76 (2), 225–251.
Wibberley, C., Shimamoto, T., 2005. Earthquake slip weakening and asperities explained by thermal pressurization. Nature, 689–692.
Wu, S., Vail, P.R., Cramez, C., 1990. Allochthonous salt, structure and stratigraphy of the north-eastern Gulf of Mexico. Part I: stratigraphy. Marine and Petroleum Geology 7 (4), 318–324. IN311-IN318, 325-332, IN319-IN316, 333.
Yasuhara, H., Elsworth, D., Polak, A., 2003. A mechanistic model for compaction of granular aggregates moderated by pressure solution. Journal of Geophysical Research-Solid Earth 108 (B11).
Zhu, W., Wong, T., 1999. Network modeling of the evolution of permeability and dilatancy in compact rock. Journal of Geophysical Research-Solid Earth, 2963–2971.